Journal of Algorithms and Computations

journal homepage: http://jac.ut.ac.ir

Numerical Simulation of PUMA560 Robotic Arm Velocity in presence of White and Colored Noise

H. Babazadeh[*,1] , P. Nabati[2] and H. Pirmohamad [2]

[1] Department of Electrical Engineering, Urmia University of Technology, Urmia, Iran

[2] Department of Science, Urmia University of Technology, Urmia, Iran

ABSTRACT

This paper presents a numerical stochastic kinematic analysis of the velocity response of a six-degree-of-freedom PUMA560 robotic manipulator under white/colored noise. Stochastic disturbances are injected directly into the joint motion functions, and the resulting linear/angular velocities of the end effector are computed using the manipulator Jacobian. White noise is modeled as the derivative of Brownian motion, while colored noise is represented by Ornstein–Uhlenbeck processes. Numerical simulations are conducted using first-, third-, and fifth-order polynomial joint trajectories, and noise effects are quantitatively evaluated using the Root-Mean-Square-Error (RMSE). The results demonstrate that higher-order joint trajectories amplify noise-induced deviations in end-effector velocity. Comparative analysis shows that the manipulator exhibits greater robustness to colored noise than to white noise. These findings provide insights for improving manipulator design and velocity accuracy under stochastic disturbances.

Keywords: Jacobian, kinematics, differential equations, angular velocity, noise

ARTICLE INFO

Article history:
Research paper
Received 17, November 2025
Accepted 01, December 2025
Available online 08, December 2025

AMS subject classification: 93C85, 93E03

[*] Corresponding author: H.Babazadeh

Email: h.babazadeh@uut.ac.ir

Journal of Algorithms and Computation 57 issue 2, December 2025, PP. 100-111

1. INTRODUCTION

Robotic manipulators are widely employed in industrial applications to reduce production costs and to perform tasks in environments that may be hazardous for human operators. To increase flexibility and dexterity, many industrial robots are designed as redundant manipulators, possessing more degrees of freedom than are strictly required for task execution. Prominent examples include the Programmable Universal Machine for Assembly (PUMA) and the Selective Compliant Articulated Robot for Assembly (SCARA), both of which are extensively used in automated manufacturing systems.

A typical robotic arm, analogous to the human arm, consists of a fixed base that provides structural support and serves as the reference coordinate frame, a sequence of rigid links connected by actuated joints, and an end effector that performs the assigned task. The coordinated motion of the joints enables the end effector to follow a prescribed trajectory with a desired position and velocity. The design and development of robotic manipulators generally begin with mechanical construction, followed by electrical integration and the implementation of control algorithms governing joint actuation [1].

In practical applications, robotic manipulators are inevitably affected by uncertainties and disturbances, which lead to deviations in the position and orientation of the end effector. Such deviations are commonly interpreted as noise and may originate from electrical components, mechanical imperfections, sensor inaccuracies, or environmental influences. These disturbances are often random and unpredictable in nature and can be effectively modeled using stochastic processes. Consequently, stochastic differential equations (SDEs) have become a valuable tool for analyzing the influence of noise on robotic systems [2].

Several studies have investigated stochastic effects in robotic and electromechanical systems. In many works, noise modeling is limited to electrical subsystems, such as motor dynamics or sensor measurements [3–6]. Data-driven approaches, including neural networks, have also been employed to estimate end-effector velocities in noisy environments [7,8]. More comprehensive studies incorporate stochastic disturbances directly into the kinematic equations of robotic manipulators; however, these are often restricted to simplified systems, such as two-link manipulators, which limit the generality of the conclusions [9].

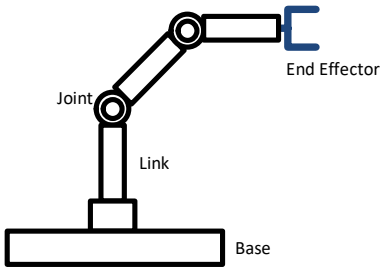

Figure 1. typical robotic arm

The PUMA560 robotic arm is a well-established six-degree-of-freedom (6-DOF) manipulator that has been extensively studied in the context of forward and inverse kinematics, trajectory planning, and control design [10–13]. Despite this extensive body of work, the effect of

general stochastic disturbances on the kinematic velocity response of the PUMA560—particularly through direct perturbation of joint motion functions—has received comparatively little attention.

In this paper, a numerical stochastic kinematic framework is proposed to analyze the linear and angular velocity of the end effector of the PUMA560 manipulator in the presence of white and colored noise. Stochastic disturbances are introduced directly into the joint angle trajectories, and the resulting end-effector velocities are computed using the Jacobian matrix. White noise is modeled as the derivative of Brownian motion, while colored noise is represented using Ornstein–Uhlenbeck processes. Although the numerical simulations are conducted on the PUMA560 robot, the proposed modeling approach is general and can be applied to other serial robotic manipulators with different geometries and degrees of freedom.

The remainder of this paper is organized as follows. Section 2 describes the physical structure and kinematic model of the PUMA560 manipulator. Section 3 presents the stochastic modeling framework for white and colored noise. Section 4 discusses the numerical simulation results for different joint trajectory orders and analyzes the influence of link length variations. Finally, Section 5 concludes the paper and outlines directions for future research.

2. PUMA ROBOT STRUCTURE

The PUMA 560 robotic manipulator, introduced in 1978, has been widely employed in industrial applications such as the assembly of automobile subcomponents. A schematic representation of the robot is provided in Fig. 2. The forward kinematic model of the manipulator is formulated using the Denavit–Hartenberg (DH) convention [1], which systematically describes the spatial relationship between successive links through a set of four parameters: $\{\alpha_{i-1},a_{i-1},d_i,\theta_i\}$, representing the twist angle, link length, link offset, and joint angle, respectively.

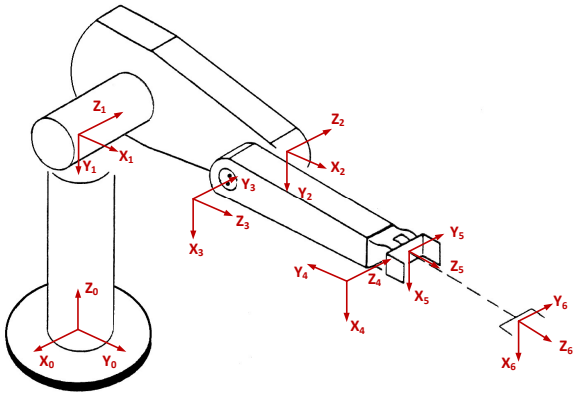

Figure 2. PUMA560 manipulator with DH based coordinates

TABLE I. DH PARAMETERS OF PUMA560

Joint i	θ_i	d_i (mm)	a_i (mm)	α_i	Range of Motion
1	θ_1	d1=660	0	-90°	-160°~160°
2	θ_2	d2=160	a2=430	0	-225°~45°
3	θ_3	d3=-10	a3= -20	90°	-45°~225°
4	θ_4	d4=433	0	-90°	-100°~170°
5	θ_5	0	0	90°	-100°~100°
6	θ_6	d6=56	0	0	-226°~226°

In accordance with the DH methodology, an orthonormal coordinate frame is assigned to each link of the manipulator, such that the transformation between adjacent frames is defined relative to the preceding one. Table 1 presents the DH parameters for the PUMA 560 robot, as specified in [14]. Based on these parameters, a homogeneous transformation matrix is computed for each joint to describe the position and orientation of the ithith frame with respect to the $(i-1)^{th}$ frame, as formulated in [15].

$$A_{i-1}^{i} = \begin{bmatrix} Cos\,\theta_i & -Cos\,\alpha_i\,Sin\,\theta_i & Sin\,\alpha_i\,Sin\theta_i & a_i Cos\theta_i \\ Sin\,\theta_i & Cos\,\alpha_i\,Cos\,\theta_i & -Sin\,\alpha_i\,Cos\theta_i & a_i Sin\theta_i \\ 0 & Sin\,\alpha_i & Cos\,\alpha_i & d_i \\ 0 & 0 & 0 & 1 \end{bmatrix} \quad (1)$$

The transformation matrices T_i, which define the position and orientation of the i_{th} coordinate frame relative to the base frame, are obtained by the sequential product of the individual homogeneous transformation matrices A_j derived from the Denavit–Hartenberg parameters. This relationship is expressed as:

$$T_0^i = A_0^1 A_1^2 \cdots A_{i-1}^i = \prod_{j=1}^{i} A_{j-1}^j = \begin{bmatrix} x_i & y_i & z_i & p_i \\ 0 & 0 & 0 & 1 \end{bmatrix}; for\ i = 1, 2, \ldots, n \quad (2)$$

where each Aj represents the homogeneous transformation from frame j−1 to frame j.

Assuming that each joint is actuated by a motor, the joint variable q(t) represents the time-dependent angular (or linear) position of the joint. As the manipulator operates, both the joint variables and the end effector's position and orientation become time-varying functions. The linear velocity **V** and angular velocity **ω** of the end effector are related to the time derivatives of the joint variables $\dot{\mathbf{q}}(\mathbf{t})$. This relationship is typically expressed through the manipulator Jacobian matrix **J(q)**, such that:

$$\xi(t) = \begin{bmatrix} V_n \\ \omega_n \end{bmatrix} = J(t) \cdot \dot{q}(t)\,. \quad J(q) = \begin{bmatrix} J_v \\ J_\omega \end{bmatrix} \quad (3)$$

$$J(q) = \begin{bmatrix} Z_0 \times (O_6 - O_0) & Z_1 \times (O_6 - O_1) & \ldots & Z_5 \times (O_6 - O_5) \\ Z_0 & Z_1 & \ldots & Z_5 \end{bmatrix} \quad (4)$$

where $\mathbf{J(q)} \in R^{6\times n}$ maps joint velocities to the end effector's spatial velocity in the base frame.

The kinematic relationship between the joint velocities and the end-effector velocities of an n-degree-of-freedom (DOF) robotic manipulator is described by the Jacobian matrix J(q). This matrix is of dimension 6×n6×n, where each column corresponds to a joint, and each row represents a component of the linear or angular velocity of the end-effector. The Jacobian depends explicitly on the physical parameters of the manipulator, such as the link lengths, as well as the specific joint variables and their configurations.

For a manipulator with six links (i.e., a six-DOF arm), the Jacobian matrix is square with dimensions 6×6. The elements of J(q) are determined by the forward kinematics and the structure of the manipulator, encapsulating both the geometry and the motion characteristics of the system.

3. STOCHASTIC MODEL

The end effector velocity is given by the formula:

$$\begin{bmatrix} V_x(t) \\ V_y(t) \\ V_z(t) \\ \omega_x(t) \\ \omega_y(t) \\ \omega_z(t) \end{bmatrix} = [J(q)]. \begin{bmatrix} \dot{q}_1(t) \\ \dot{q}_2(t) \\ \dot{q}_3(t) \\ \dot{q}_4(t) \\ \dot{q}_5(t) \\ \dot{q}_6(t) \end{bmatrix} \quad (5)$$

Where $\dot{q}_i(t) = \dot{\theta}_i(t)$ since all joints are revolute, and J(q), the Jacobean matrix, is calculated using relation (4).

The joint angle functions are determined using path detection or motion detection methods for robotic manipulators. These functions are typically defined as polynomials of various orders, taking into account position, velocity, or acceleration constraints at the start and end points of the end effector's trajectory [16]. In this study, first-, third-, and fifth-order polynomial equations are analyzed for all joints.

While this study focuses on white and Ornstein–Uhlenbeck noise, the framework can be adapted to other stochastic processes.

A. White Noise Stochastic Model

White noise, also known as random noise, is a type of stochastic signal characterized by equal intensity across all frequencies within a specified bandwidth. It is defined by statistical properties including a zero mean and a constant power spectral density (PSD). To analyze the effect of white noise, the joint angle function equations are modified as follows:

$$\theta_i^*(t) = \theta_i(t) + \text{"white noie"} = \theta_i(t) + \sigma_i \omega_i(t) \quad (6)$$

Where σi is a positive constant representing the noise intensity, and ωi(t) is an Ft-adapted white noise process defined on the underlying probability space (Ω,F,P), which is supported by a right-continuous filtration {Ft,t≥0}. Since white noise can be interpreted as the generalized derivative of Brownian motion, ωi(t) can be replaced by the differential dBi(t) in equation (6), yielding:

$$\begin{bmatrix} V_x(t) \\ V_y(t) \\ V_z(t) \\ \omega_x(t) \\ \omega_y(t) \\ \omega_z(t) \end{bmatrix} = [J(\theta)]. \begin{bmatrix} \dot{\theta}_1(t) + \sigma_1 dB_1(t) \\ \dot{\theta}_2(t) + \sigma_2 dB_2(t) \\ \dot{\theta}_3(t) + \sigma_3 dB_3(t) \\ \dot{\theta}_4(\beta t) + \sigma_4 dB_4(t) \\ \dot{\theta}_5(t) + \sigma_5 dB_5(t) \\ \dot{\theta}_6(t) + \sigma_6 dB_6(t) \end{bmatrix} \quad (7)$$

where B(t) is a one-dimensional Brownian motion.

B. Colored Noise Stochastic Model

In contrast to white noise, colored noise is a random signal characterized by varying intensities across different frequencies within a specified bandwidth, resulting in a non-uniform power spectral density (PSD). Colored noise is modeled as an Ornstein–Uhlenbeck process, which satisfies the following linear additive stochastic differential equation (SDE):

$$\begin{cases} d\beta(t) = -\lambda\beta(t)dt + \sigma dB(t) \\ \beta(0) = \beta_0 \end{cases} \quad (8)$$

Where β(t) denotes the colored noise process, λ and σ are positive constants, and β_0 is a random variable independent of the standard Brownian motion. According to [18], the stochastic differential equation admits a unique strong solution given by:

$$\beta(t) = \exp(-\lambda t)(\beta_0 + \sigma \int_0^t \exp(\lambda s)\, dB(s)) \quad (9)$$

the angle function equations can be rewritten as:

$$\theta_i^*(t) = \theta_i(t) + \text{"colored noie"} = \theta_i(t) + \sigma_i \beta_i(t) \quad (10)$$

and the relation (7) will be as follows in the case of colored noise:

$$\begin{bmatrix} V_x(t) \\ V_y(t) \\ V_z(t) \\ \omega_x(t) \\ \omega_y(t) \\ \omega_z(t) \end{bmatrix} = [J(\theta)]. \begin{bmatrix} \dot{\theta}_1(t) + \sigma_1 d\beta_1(t) \\ \dot{\theta}_2(t) + \sigma_2 d\beta_2(t) \\ \dot{\theta}_3(t) + \sigma_3 d\beta_3(t) \\ \dot{\theta}_4(t) + \sigma_4 d\beta_4(t) \\ \dot{\theta}_5(t) + \sigma_5 d\beta_5(t) \\ \dot{\theta}_6(t) + \sigma_6 d\beta_6(t) \end{bmatrix} \quad (11)$$

In both white/colored noise cases, the amplitude of linear (V) and angular(ω) velocity vectors can be calculated as:

$$V(t) = \sqrt{V_x(t)^2 + V_y(t)^2 + V_z(t)^2}$$
$$\omega(t) = \sqrt{\omega_x(t)^2 + \omega_y(t)^2 + \omega_z(t)^2} \quad (12)$$

4. SIMULATION RESULTS

Numerical methods have been developed to approximate solutions for certain stochastic differential equations (SDEs), as closed-form analytical solutions are generally unavailable . Consider the time interval [0,T] partitioned into nn equal subintervals defined by the points $\{0,t_1,t_2,\ldots,t_n=T\}$, where nn is a positive integer and $\Delta t=T/n$. In the initial step, the colored noise process is simulated using the Euler–Maruyama scheme applied to equation (8):

$$\beta(t_i + 1) = \beta(t_i) - \lambda\beta(t_i)\Delta t + \sigma\Delta B(t_i), \tag{13}$$

$$\Delta B(t_i) = B(t_{i+1}) - B(t_i) \sim N(0, \Delta t) \tag{14}$$

By setting n=1000, the simulated values of $\beta(t_i)$ can be generated using Python code. Subsequently, the discrete Euler method is employed to simulate equations (7) and (11).

To define the joint angle functions, the initial and final boundary conditions of the robotic arm must be taken into account. In the simplest case, where only position constraints are considered, a first-order polynomial is sufficient.

$$\theta_i(t) = at + b \tag{15}$$

Where b represents the initial joint angle and aa denotes the rate of increment. For a comprehensive analysis of the manipulator, a duration of 10 seconds is selected for each joint to move through its full range, from the initial to the final angle, as specified in the last column of Table 1. Accordingly, the joint angle functions can be expressed as follows:

$$\begin{aligned}
\theta_1(t) &= 32t - 160 \\
\theta_2(t) &= 27t - 225 \\
\theta_3(t) &= 27t - 45 \\
\theta_4(t) &= 27t - 100 \\
\theta_5(t) &= 20t - 100 \\
\theta_6(t) &= 45.2t - 226
\end{aligned} \tag{16}$$

When both initial and final velocities are considered, third-order polynomials are employed to define the joint angle functions. To reduce complexity, the initial velocity of each joint angle is set to zero, while the final velocity is assigned a value of 10. Under these conditions, the joint angle functions are expressed as follows:

$$\begin{aligned}
\theta_1(t) &= 0.54t^3 - 7.6t^2 - 160 \\
\theta_2(t) &= 0.44t^3 - 6.1t^2 - 225 \\
\theta_3(t) &= 0.44t^3 - 6.1t^2 - 45 \\
\theta_4(t) &= 0.44t^3 - 6.1t^2 - 100 \\
\theta_5(t) &= 0.3t^3 - 4t^2 - 100 \\
\theta_6(t) &= 0.804t^3 - 11.56t^2 - 226
\end{aligned} \tag{17}$$

In the subsequent case, acceleration constraints are incorporated, resulting in joint angle functions represented by fifth-order polynomials. The initial acceleration is set to zero, while the final acceleration is assigned a value of one. Thus, the joint functions are defined as follows:

$$\begin{aligned}
\theta_1(t) &= 0.0167t^5 - 0.42t^4 + 2.85t^3 - 160 \\
\theta_2(t) &= 0.0137t^5 - 0.345t^4 + 2.35t^3 - 225 \\
\theta_3(t) &= 0.0137t^5 - 0.345t^4 + 2.35t^3 - 45 \\
\theta_4(t) &= 0.0137t^5 - 0.345t^4 + 2.35t^3 - 100 \\
\theta_5(t) &= 0.0095t^5 - 0.24t^4 + 1.65t^3 - 100
\end{aligned} \tag{18}$$

$$\theta_6(t) = 0.04982t^5 - 0.618t^4 + 4.17t^3 - 226$$

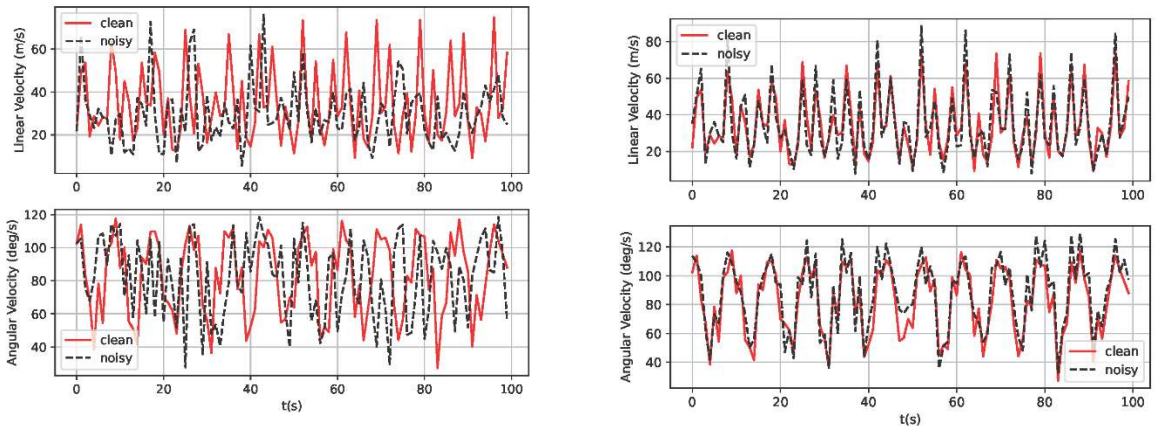

(a) (b)

Figure 3 Linear and angular velocity of the end effector in presence of (a) white noise, (b) colored noise for 1st order joint functions

For the simulations, each set of the previously described equations is evaluated independently. In each scenario, white and colored noise profiles with an intensity of 0.5 are introduced. The physical lengths of the manipulator links are assigned based on the specifications provided in Table 1.

Figure 3 presents the simulation results for the first-order polynomial equations under both white and colored noise conditions. The linear and angular velocities of the end effector are illustrated. Figures 4 and 5 depict the corresponding results for the third- and fifth-order polynomial equations, respectively. In each simulation, the root mean square error (RMSE) between the results with and without noise was calculated. The analysis reveals that the impact of noise intensifies as the polynomial order increases.

The robotic arm demonstrates greater tolerance to colored noise compared to white noise, as evidenced by the closer alignment between the velocity profiles with and without noise in the presence of colored noise.

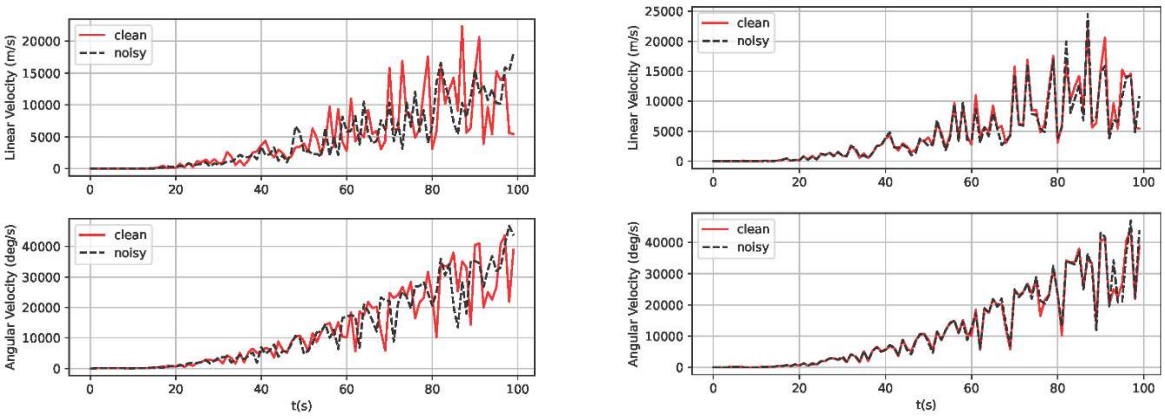

Figure 4 Linear and angular velocity of the end effector in presence of (a) white noise, (b) colored noise for 3rd order joint functions

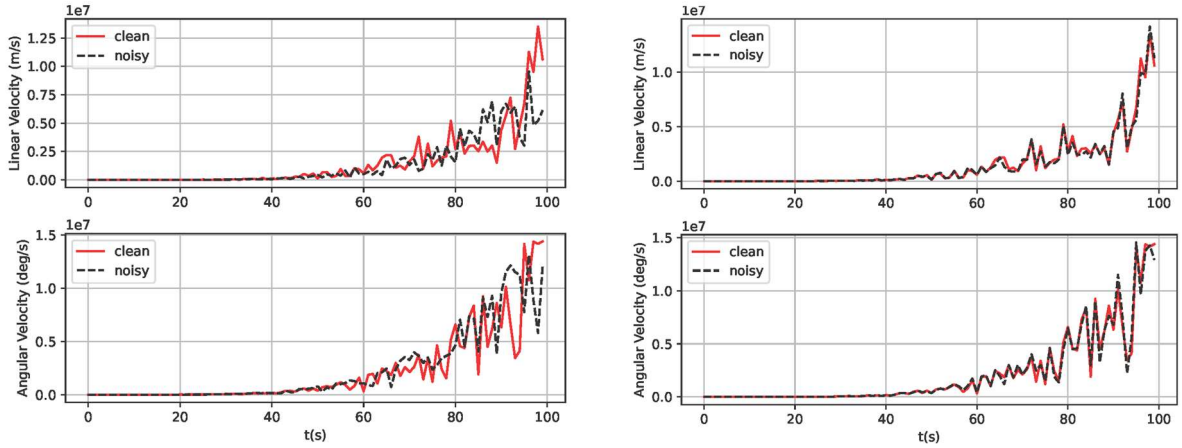

Figure 5 Linear and angular velocity of the end effector in presence of (a) white noise, (b) colored noise for 5rd order joint functions

Beyond the joint functions, the physical structure of the robot plays a critical role when operating in noisy environments. Typically, the design of a manipulator is based on its forward and inverse kinematic equations. Once implemented, the link lengths are fixed and cannot be altered; therefore, their potential impact on overall system performance must be considered during the design phase.

To investigate this effect, simulations were conducted to assess how variations in link lengths influence the end-effector velocity under noisy conditions. Specifically, the link parameters d_1, a_2, a_3, and d_4 of the PUMA robot (as listed in Table 1) were varied over the range from 0 to 100 cm. The joint angle functions were modeled as third-order polynomials. The root

mean square error (RMSE) between the noise-free and noisy end-effector velocities was computed for both linear and angular components, with noise intensity set to 0.5 for both white and colored noise. Figures 6 and 7 illustrate these results, showing that the deviation in linear velocity increases with link length, whereas the angular velocity remains largely unaffected. These findings indicate that minimizing link lengths is advantageous for reducing perturbations in the end-effector's linear velocity under noisy operating conditions.

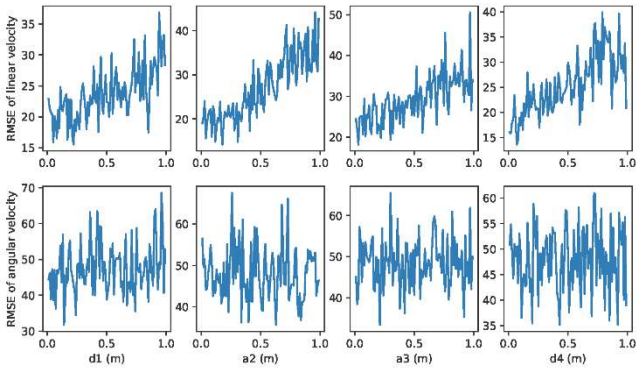

Figure 6 RMSE of Linear and angular velocity of end effector versus different links with and without white noise

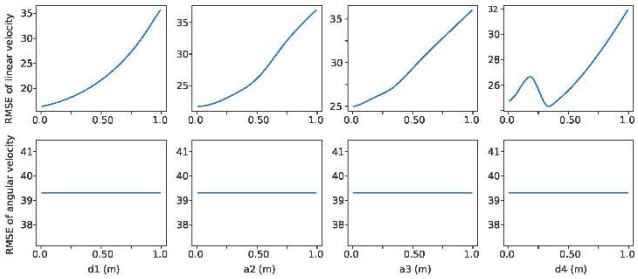

Figure7 RMSE of Linear and angular velocity of end effector versus different links with and without colored noise

5. CONCLUSION

This study presented a numerical stochastic kinematic analysis of the 6-DOF PUMA560 robotic manipulator to investigate the influence of stochastic disturbances on the linear and angular velocity of the end effector. By injecting white and colored noise directly into the joint motion functions and computing the resulting velocities through the Jacobian matrix, a general and systematic framework for noise analysis in robotic manipulators was developed. Numerical simulations based on first-, third-, and fifth-order polynomial joint trajectories demonstrated that higher-order trajectories lead to increased sensitivity to stochastic disturbances, as quantified using the root mean square error (RMSE).

A comparative analysis showed that colored noise, modeled using Ornstein–Uhlenbeck processes, induces smaller velocity deviations than white noise, indicating greater robustness of the manipulator under temporally correlated disturbances. In addition, the structural sensitivity study revealed that increasing link lengths significantly amplifies perturbations in the linear velocity of the end effector, while the angular velocity remains largely unaffected. These findings

emphasize the importance of considering both trajectory smoothness and physical dimensions during manipulator design, particularly for applications requiring high precision in noisy environments.

It should be noted that the results presented in this study are based solely on numerical simulations, and no experimental validation using physical robotic hardware was performed. Experimental implementation and validation on real robotic platforms therefore constitute an important direction for future work. Further extensions may include the incorporation of additional noise models, dynamic effects, and advanced filtering or control strategies to mitigate the impact of stochastic disturbances. Although the numerical examples focus on the PUMA560 manipulator, the proposed stochastic kinematic framework is applicable to a wide class of serial robotic arms.

REFERENCES

[1] Spong, Mark W., Seth Hutchinson, and Mathukumalli Vidyasagar. “Robot modeling and control”. John Wiley & Sons, 2020.

[2] Evans, Lawrence C. “An introduction to stochastic differential equations”. Vol. 82. American Mathematical Soc., 2012.

[3] Farnoosh, Rahman, Parisa Nabati, Ramazan Rezaeyan, and Morteza Ebrahimi. "A stochastic perspective of RL electrical circuit using different noise terms." COMPEL-The international journal for computation and mathematics in electrical and electronic engineering 30, no. 2 (2011): 812-822.

[4] Farnoosh, Rahman, Parisa Nabati, and A. Hajirajabi. "Parameters estimation for RL electrical circuits based on least square and Bayesian approach." COMPEL-The international journal for computation and mathematics in electrical and electronic engineering 31, no. 6 (2012): 1711-1725.

[5] Nabati, Parisa, Hadiseh Babazadeh, and Hamed Azadfar. "Noise analysis of band pass filters using stochastic differential equations." COMPEL-The international journal for computation and mathematics in electrical and electronic engineering 38, no. 2 (2019): 693-702.

[6] Ahn, Min Sung, Hosik Chae, Donghun Noh, Hyunwoo Nam, and Dennis Hong. "Analysis and noise modeling of the intel realsense d435 for mobile robots." In 2019 16th International Conference on Ubiquitous Robots (UR), pp. 707-711. IEEE, 2019.

[7] Yildirim, Şahin, and İkbal Eski. "Noise analysis of robot manipulator using neural networks." Robotics and Computer-Integrated Manufacturing 26, no. 4 (2010): 282-290.

[8] Jin, Long, Shuai Li, Lin Xiao, Rongbo Lu, and Bolin Liao. "Cooperative motion generation in a distributed network of redundant robot manipulators with noises." IEEE Transactions on Systems, Man, and Cybernetics: Systems 48, no. 10 (2017): 1715-1724.

[9] Babazadeh, Hadiseh, and Parisa Nabati. "Numerical simulation of two link robotic manipulator with white and colored noise." Computational Methods for Differential Equations 12, no. 1 (2024): 149-158.

[10] Corke, Peter I., and Brian Armstrong-Helouvry. "A search for consensus among model parameters reported for the PUMA 560 robot." In Proceedings of the 1994 IEEE International Conference on Robotics and Automation, pp. 1608-1613. IEEE, 1994.

[11] Lavín-Delgado, J. E., J. E. Solís-Pérez, J. F. Gómez-Aguilar, and R. F. Escobar-Jiménez. "Trajectory tracking control based on non-singular fractional derivatives for the PUMA 560 robot arm." Multibody System Dynamics 50, no. 3 (2020): 259-303.

[12] Al Mashhadany, Yousif I. "Virtual reality trajectory of modified PUMA 560 by hybrid intelligent controller." Bulletin of Electrical Engineering and Informatics 9, no. 6 (2020): 2261-2269.

[13] Singh, Gurjeet, Vijay Kumar Banga, and Thaweesak Yingthawornsuk. "Inverse Kinematics Solution of Programmable Universal Machine for Assembly (PUMA) Robot." In 2019 15th International Conference on Signal-Image Technology & Internet-Based Systems (SITIS), pp. 518-524. IEEE, 2019.

[14] Shen, Wei. "Kinematics Analysis and Trajectory Planning of Robot Based on MATLAB." In 2021 IEEE International Conference on Power Electronics, Computer Applications (ICPECA), pp. 895-897. IEEE, 2021.

[15] Lee, C. S. G., and M. Ziegler. "Geometric approach in solving inverse kinematics of PUMA robots." IEEE Transactions on Aerospace and Electronic Systems 6 (1984): 695-706.

[16] Mei, Tianxiang, Yi Yang, Jianbo Chen, Zhang Guihong, Ziyun Jiao, Long Gao, Xiaolin Ren, and Qing Li. "Simulation Research on Motion Trajectory of PUMA 560 Manipulator Based on MATLAB." In 2019 Chinese Control And Decision Conference (CCDC), pp. 4857-4862. IEEE, 2019.

[17] Nabati, Parisa. "A simulation study of the COVID-19 pandemic based on the Ornstein-Uhlenbeck processes." Computational Methods for Differential Equations 10, no. 3 (2022): 738-745.

[18] Babazadeh, Hadiseh, and Parisa Nabati. "Numerical simulation of two link robotic manipulator with white and colored noise." Com